Z. Angew. Math. Phys. (2019) 70:9

0044-2275/19/010001-17
published online November 29, 2018
https://doi.org/10.1007/s00033-018-1055-1

Zeitschrift für angewandte Mathematik und Physik ZAMP

A model for bone mechanics and remodeling including cell populations dynamics

Alessio Ciro Rapisarda, Alessandro Della Corte, Rafał Drobnicki, Fabio Di Cosmo and Luigi Rosa

Abstract. In this paper, we propose a model for the description of bone mechanics and bone remodeling processes, including bone cell populations dynamics. The latter, described by a system of ODEs, influences the values for the elastic parameters used in the mechanical model, which in turn determines the "stimulus" function affecting the behavior of the cells. Numerical simulations concerning the behavior of the bone under external loads, as well as simple fracture healing processes are presented. The model can reproduce the qualitative behavior of bone tissue remodeling and mechanical response.

Mathematics Subject Classification. 74F99, 74B99.

Keywords. Bone tissue, Bone remodeling, Cell populations dynamics, Numerical simulations of bone mechanics.

1. Introduction

In this paper, we present and numerically investigate a mathematical model aiming to describe some bio-mechanical phenomena which occur in bone tissues. The studies on the bone remodeling were started in the nineteenth century and are still ongoing, and especially in the last years the role of mathematical modeling has increased significantly (see for instance [5,28,31,34,35]). However, the process of bone remodeling is not completely understood yet, especially because of the complexity of the skeletal system and its interactions with the other parts of the body, which limits the capability of a single model to capture all of the relevant biological, biochemical and biophysical mechanisms occurring at all time and space scales simultaneously.

Let us briefly recall that three populations of cells are mainly responsible for bone remodeling: *osteoblasts*, which produce new bone tissue, *osteoclasts*, which resorb bone tissue, and *osteocytes*, which (roughly speaking) are able to sense mechanical stimuli and communicate with the other cells. We also recall that osteoblasts derive from mesenchymal stem cells, osteoclasts derive from monocyte differentiation, while osteocytes derive from osteoblasts that have been completely surrounded by the bone tissue they produced.

As already said, many things are still unclear from a purely biological point of view. In particular, concerning cell populations dynamics in bones, some important things that are still unclear are (see [17]):

- Whether the decision for an osteoblast to become an osteocyte is dictated by a specific pattern of gene expression in a subset of osteoblasts.
- Whether this is a cell autonomous response or one that is controlled via the surface cells receiving signals from already embedded osteocytes.
- Whether every osteoblast has an equal chance of becoming an osteocyte or whether there are specific subpopulations with predefined fates.
- Whether osteocytic differentiation is an irreversible process or whether osteocytes have the capacity to revert to being an osteoblast or even give rise to other cell lineages, such as adipocytes and chondrocytes.

The main idea presented herein is to introduce a system of ODEs accounting for the description of cell populations dynamics. The solution of this system, at every time step, provides the values for the mechanical parameters used in the mechanical model, which in turn determines the "stimulus" function which affects cells' behavior. The two legs of the model, the nondimensional ODEs describing cells and the mechanical model describing the physical behavior of the bone, are therefore strongly interconnected, which naturally arises from the complex nature of the biological phenomena under investigation: there is a two-way game between *macro* and *micro*, as both levels influence the other one.
Of course in the model, a number of assumption will be made for the sake of simplicity, as the main aim is to reach a suitable compromise between the capability of the model to describe the interested phenomena and its manageability and understandability. A complete and simultaneous description of all the phenomena occurring in bone growth or resorption may lead to models too complex to be reasonable at this stage of the research. Our intended research line consists instead of a step by step refining of the basic model here presented. The results from this first stage will pave the way for different kinds of generalizations. In particular, we expect that, in order to account for the complexity of the geometry of the bone at the microscale, more complex mechanical models suitable for microstructured continua could be efficiently used. Micromorphic continua are, indeed, used for the modeling of both natural materials (see for instance [29,30,33,40,48]) and materials with artificial microstructure (see for instance [2–4,10,13,23–25,41]). Moreover, the introduction of higher gradient continuum models can also be useful as the geometrically rather ordered structure of the trabeculae can produce typical higher gradient effects (see [1,6,9,20,21,27]).

2. The model

The mechanical component of the model is based on [35]. This model will be enriched with the results from [28,31,34].

2.1. Assumptions

The key assumptions of the model are the following:

- The elastic properties of the bone tissue are described by means of an isotropic Cauchy continuum in small deformations regime.
- The communication between the sensor and actor cells is modeled by means of a scalar field called *Stimulus* and denoted by S, defined at every point of the bone and depending on the overall mechanical load (suitably weighted by the distance between the point where S is evaluated and the source of the signal, as we will see) and on the density of sensor cells.
- The status of the system at a given time is given by the macro-mechanical variables as well as the *internal* state, i.e., the scalar fields representing the cells densities;
- The timescale is so large that no inertial effects have to be taken into account.
- The timescale is such that loading has to be intended as averaged on a suitably long period.
- The precursor cells are indefinitely available.

The main novelty of the presented cell populations dynamics model (introduced in a simplified form in [19]) is the introduction of the osteocytes (which are not present, for instance, in [34]). Most of recent biological discoveries concern indeed the role of osteocytes. There has been experimental proof of their essential role in the maintenance of mineralized bone, and there is clear evidence that osteocytes influence population dynamics through several different signal transduction pathways. In particular, in addition to already known cytokines, the role of WNT (Wingless-related integration site) signaling pathways has been discovered (see, e.g., [50,51]).

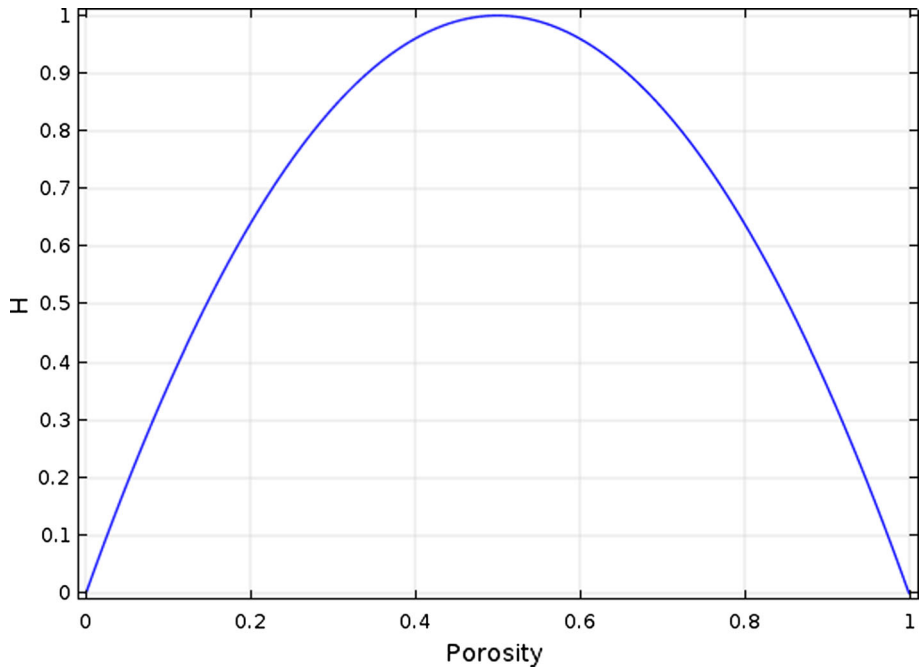

FIG. 1. Plot of the function $H(\varphi)$

Therefore, our model is designed in order to take into account:

- Cell differentiation from progenitor cells to osteoblasts and osteoclasts.
- Cell differentiation from osteoblasts to osteocytes.
- The role of mechanical stimulus.
- The multiplicity of signaling pathways between osteocytes and other cell populations.

2.2. The ODEs system

The proposed system of ODEs describing the time evolution of cell densities and bone tissue density is:

$$\frac{\partial x_k}{\partial t} = -\beta_k X_k + \gamma_{bk} x_b \mathcal{K}(\varphi) \tag{1}$$

$$\frac{\partial x_b}{\partial t} = -\beta_b X_b - \gamma_{bk} x_b \mathcal{K}(\varphi) + \alpha_b S^+ x_k \tag{2}$$

$$\frac{\partial x_c}{\partial t} = -\beta_c X_c + \gamma_c x_c \mathcal{K}(\varphi) + \alpha_c S^- x_k \tag{3}$$

$$\frac{\partial \rho}{\partial t} = (a x_b - b x_c) H(\varphi) \tag{4}$$

The terms x_k, x_b, x_c indicate, respectively, the density of osteocytes, osteoblasts and osteoclasts. The terms X_k, X_b, X_c are defined by:

$$X_i = \begin{cases} x_i, & \text{if } x_i > \tilde{x}_i \\ 0, & \text{if } x_i \leqslant \tilde{x}_i \end{cases}$$

where i can be k, b or c.

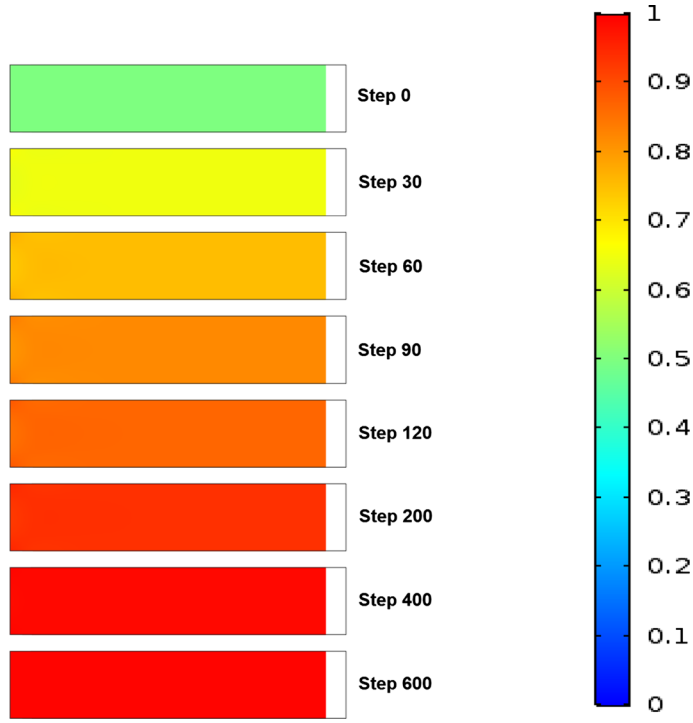

FIG. 2. A rectangular bone sample under simple compressive load. In color map, the (apparent) density of bone tissue is indicated. The external rectangle represents the unstressed configuration of the sample (color figure online)

The terms $-\beta_k$, $-\beta_b$, $-\beta_c$ indicate the removal rate of the cells (mainly due to apoptosis). The presence of the variables X_i entails that the removal begins over a certain density threshold ($\tilde{x}_i$). Here, β_k, β_b, β_c are supposed constant. The terms $-\gamma_{bk}x_b\mathcal{K}(\varphi)$ and $+\gamma_{bk}x_b\mathcal{K}(\varphi)$ describe the differentiation from osteoblasts to osteocytes. The γ_{bk} parameter is assumed constant, while instead $\mathcal{K}$ is a function of the porosity that will be discussed in the next section. The term $+\gamma_c\mathcal{K}(\varphi)$ models the birth and activation by osteoclasts and is again depending on the function $\mathcal{K}$, while γ_c is a constant parameter. The terms $+\alpha_b S^+ x_k$ and $+\alpha_c S^- x_k$ model the creation of osteoblasts and osteoclasts due, respectively, to large or small values of the stimulus. Indeed, S^+ denotes of course the positive part of S (which tends to activate osteoblasts), while S^- the negative part (which tends to activate osteoclasts). As we will see, the density of osteocytes x_k also appears in the definition of the stimulus (see Eq. (6)). In this way, we account for at least two different signaling pathways between osteocytes and other cell populations: one is directly related to the density of cells, the other takes into account that the density of osteocytes can amplify the stimulus. The two parameters α_b and α_c are assumed constants.

The apparent density of bone tissue, i.e., the average mass density over a REV large enough to make it sensible to homogenize the porous structure of the bone, is denoted by ρ. In the time derivative of ρ, there are two parameters, a and b, which represent the synthesis and resorption rate for a single osteoblast/osteoclast. They are assumed constants. The variable φ indicates the porosity. The function H is designed in order to account for the influence of effective porosity on the biological activity of cells: when the effective porosity is too large there is not enough material on which actor cells may stay, while when it is too small there is not enough free space in the pores to allow their mobility and deposit. The function $H(\varphi)$ is modeled with a parabola. The function used herein is:

$$H(\varphi) = H(1-\rho) = 4(1-\rho)\rho. \tag{5}$$

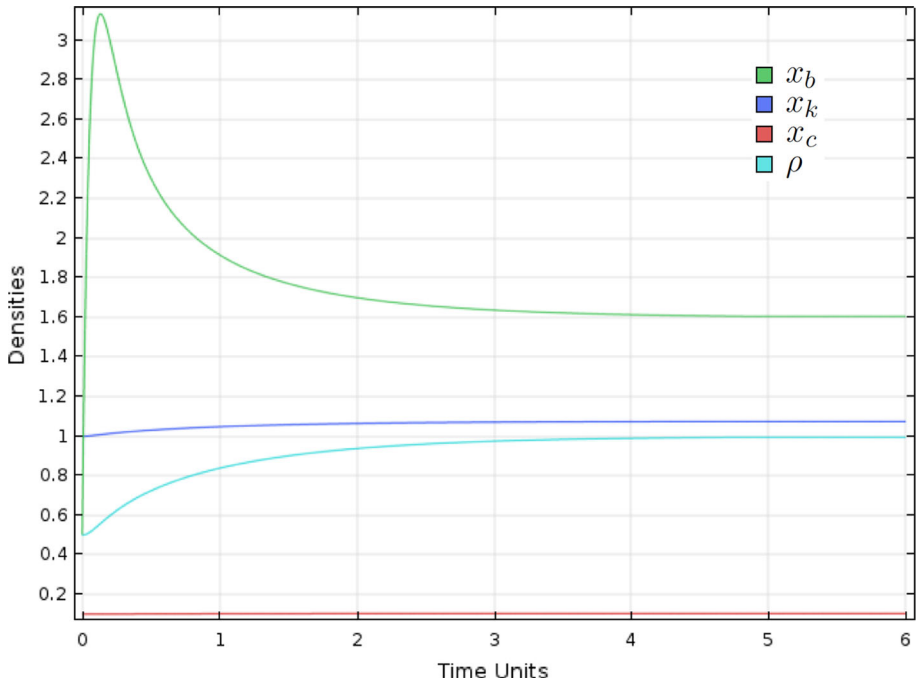

FIG. 3. Cell populations dynamics and density for a rectangular bone sample under simple compressive load. The values of the variables are evaluated at the central point of the sample. The picture shows the time history of the cell densities and bone tissue density. In green is shown the osteoblasts density, in blue the osteocytes density, in red the osteoclasts density and in cyan the bone tissue density (color figure online)

2.3. The stimulus function

The stimulus function is defined as:

$$S(x,t) = \left(\frac{\int_{\mathcal{B}} U(y,t)\eta x_k(y,t) e^{-\frac{\|x-y\|^2}{2D^2}}\, dy}{\int_{\mathcal{B}} e^{-\frac{\|x-y\|^2}{2D^2}}\, dy} \right) - S_0(x,t). \tag{6}$$

Here, $\mathcal{B}$ is the reference configuration of the bone sample, $U(x,t)$ is the deformation energy density at point $x \in \mathcal{B}$ and time t, η is a parameter measuring how much the stimulus is affected by the density of sensor cells, and D measures the range of action of sensor cells. The denominator is a normalization factor introduced in order to avoid that the outermost material points are less influential than those found inside the body only because they have less material points around (see [31]). Finally, S_0 is a positive function representing the reference value for the stimulus, associated with a physiological amount of loading (different from zero), which entails a biological equilibrium state in which the effect of resorption and synthesis is balanced. In fact if $U = 0$ then $S = -S_0$, which will enhance the action of the osteoclasts. That accounts for bone tissue impoverishment caused by long periods of rest or low loading (as in the case of astronauts living in low-gravity environments for long periods). In the paper, we will consider S_0 as constant and uniform, and the corresponding value will be chosen so that a steady state for the bone tissue and cell populations densities is obtained.

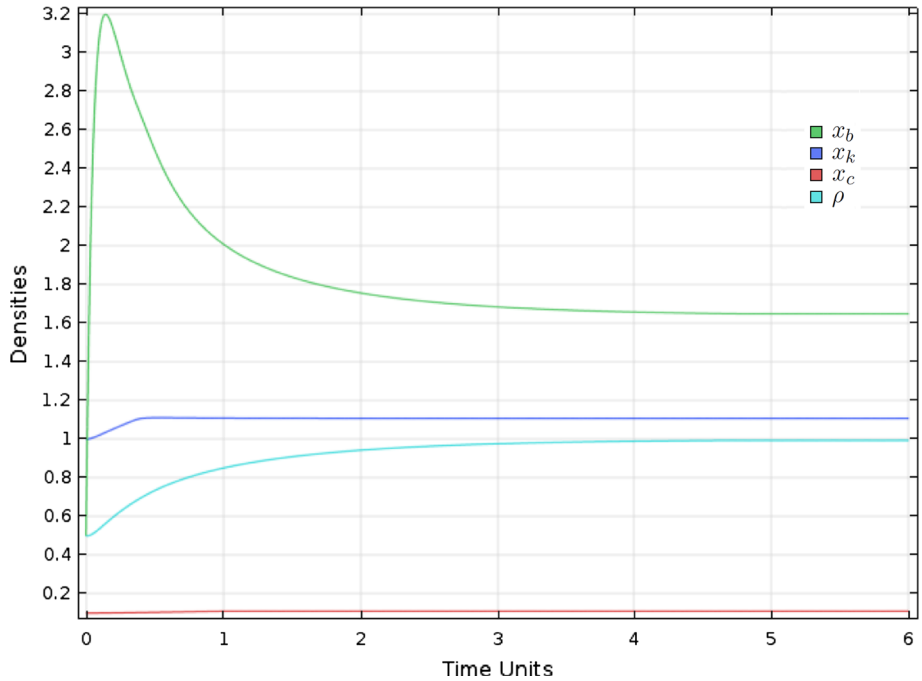

FIG. 4. Cell populations dynamics and density for a rectangular bone sample under simple compressive load. The values of the variables are evaluated at the central point of the sample. The picture shows the time history of the cell densities and bone tissue density. This time the function $\mathcal{K}(\rho)$ was $\mathcal{K} \equiv 1$, which means that the amount of porosity has less effect on the cell populations dynamics. In green is shown the osteoblasts density, in blue the osteocytes density, in red the osteoclasts density and in cyan the bone tissue density (color figure online)

2.4. The function $\mathcal{K}(\varphi)$

The function $\mathcal{K}(\varphi)$ deserves a special attention. In general, one may suppose that the function $\mathcal{K}(\varphi)$ can change between Eqs. (1), (2) and (3), but for the sake of simplicity we started by considering just one function for the three ODEs. We used again a parabola, like the function H shown before, since if the bone is too dense or too rare the activity of the actor cells is stopped or hindered. A more realistic form of this function is left to future investigation.

The constitutive equation for the porosity is:

$$\varphi = 1 - \theta \frac{\rho}{\rho_{\max}} \quad , \quad 0 < \theta \leqslant 1 \tag{7}$$

just like in [7,35] and [8]. For simplicity, we set $\rho_{\max} = \theta = 1$. The relation between the porosity and the bone density is:

$$\varphi = 1 - \rho. \tag{8}$$

Unless differently specified, the function $\mathcal{K}(\varphi)$ used in the simulations is:

$$\mathcal{K}(\varphi) = \mathcal{K}(1 - \rho) = 4(1 - \rho)\rho. \tag{9}$$

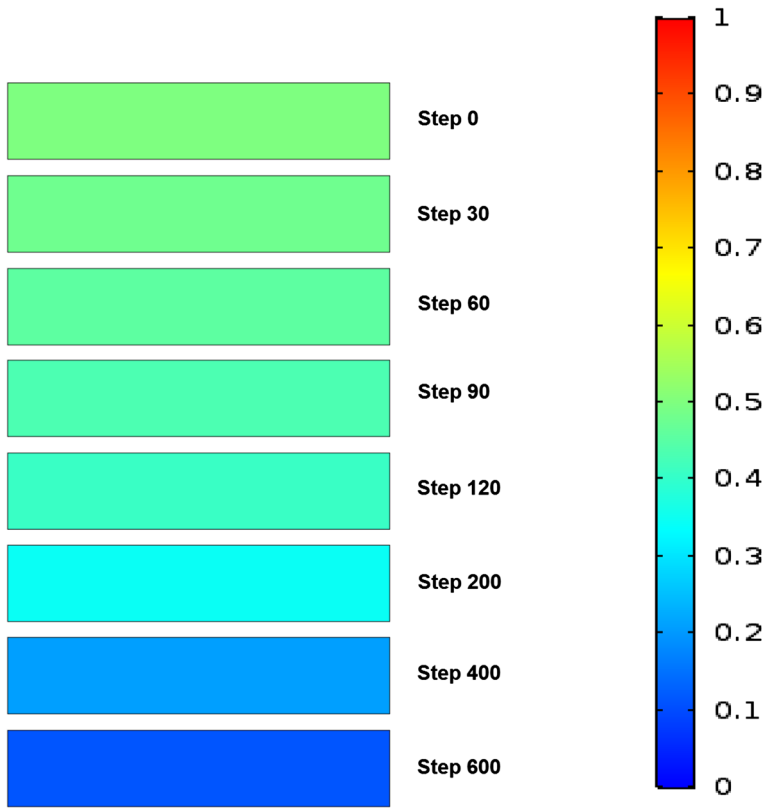

FIG. 5. A rectangular bone sample in absence of loading. In color map, the (apparent) density of bone tissue is indicated. It can be seen that the density decreases, as is to be expected in a long period of absence or very limited physical activity (color figure online)

2.5. The mechanical model

The deformation gradient ($\boldsymbol{F}$), its determinant (J) and the Green–Saint–Venant strain tensor ($\boldsymbol{G}$) are defined as usual:

$$\boldsymbol{F} = \nabla \boldsymbol{\chi}, \qquad J = \det \boldsymbol{F}, \qquad 2\boldsymbol{G} = \boldsymbol{F}^T \boldsymbol{F} - \boldsymbol{I}, \tag{10}$$

where $\boldsymbol{\chi} : \mathcal{B} \to \mathbb{R}^3$ is the placement function.
It has been assumed that the deformation energy density can be expressed as a function of the Green–Saint–Venant strain tensor, the apparent volume Lagrangian mass densities and the position of the considered material particle. It has to be noted that the assumed deformation energy does not depend explicitly on time and that the mass of the object changes very slowly in time. As already said, the timescale is assumed slow enough that no inertia effects need to be taken in account, so that the behavior can be considered quasi-static. In formulas, it is assumed the existence of a function U, representing the strain energy, such that

$$U(\boldsymbol{G}, \rho, x) = \mu \mathrm{tr}(\boldsymbol{G}^2) + \frac{\lambda}{2}(\mathrm{tr}(\boldsymbol{G}))^2. \tag{11}$$

where μ and λ are the Lamé parameters. Since the material is not homogeneous, and its density evolves with the time, μ and λ are assumed as depending on t and x. Thus:

$$\mu = \hat{\mu}(\rho, x), \quad \lambda = \hat{\lambda}(\rho, x). \tag{12}$$

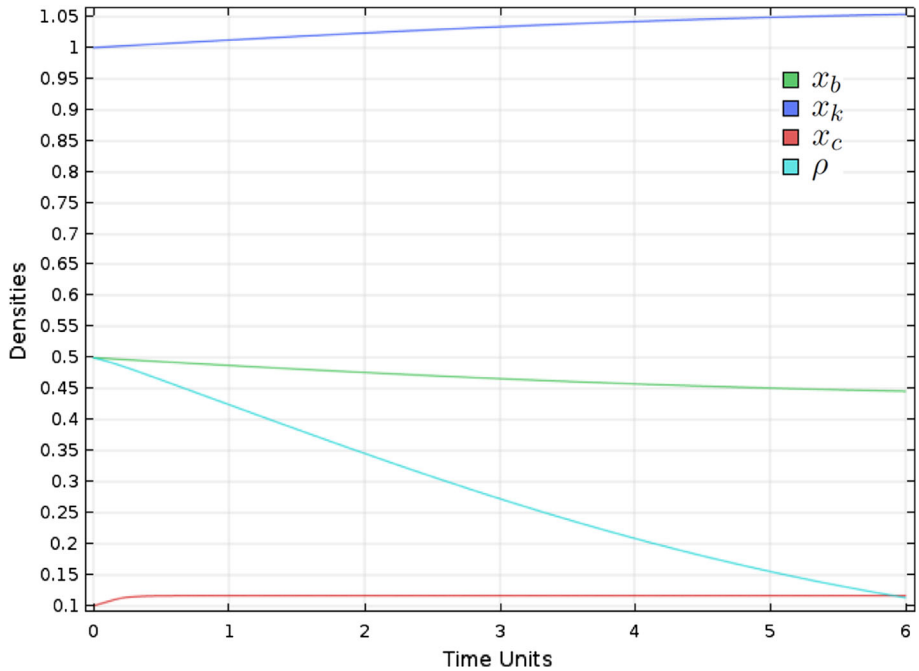

FIG. 6. Cell populations dynamics and density for a rectangular bone sample in absence of loading. The values of the variables are evaluated at the central point of the sample. The picture shows the time history of the cell densities and bone tissue density. In green is shown the osteoblasts density, in blue the osteocytes density, in red the osteoclasts density and in cyan the bone tissue density (color figure online)

For our aims, it will be handy to use Young's modulus and Poisson ratio, related to Lamé parameters by the well-known relations:

$$\lambda = \frac{Y\nu}{(1+\nu)(1-2\nu)}, \tag{13}$$

$$\mu = \frac{Y}{2(1+\nu)} \tag{14}$$

where Y is the Young modulus, ν is the Poisson ratio. The Young modulus for the bone tissue is assumed to be:

$$Y = Y_m \left(\frac{\rho}{\rho_{max}}\right)^c, \tag{15}$$

where ρ_{max} is the maximum value possible for ρ and Y_m is the maximum value for the Young modulus, while c is a parameter.

The mechanical equilibrium of the sample is governed by the usual balance equations:

$$\mathrm{Div}\boldsymbol{T} = \mathrm{Div}\left(\boldsymbol{F}\cdot\frac{\partial U}{\partial \boldsymbol{G}}\right) = -\boldsymbol{b}^{ext}, \tag{16}$$

$$\boldsymbol{T}[\boldsymbol{N}] = \boldsymbol{F}\cdot\frac{\partial U}{\partial \boldsymbol{G}}\cdot\boldsymbol{N} = \boldsymbol{f}^{ext}, \tag{17}$$

where $\boldsymbol{T}$ is the first Piola stress tensor. Equation (16) gives the force $(-\boldsymbol{b}^{ext})$ acting on a representative elementary volume of the considered sample, while eq. (17) gives the force acting on the unity surface $(\boldsymbol{f}^{ext})$ (with outward unit normal $\boldsymbol{N}$).

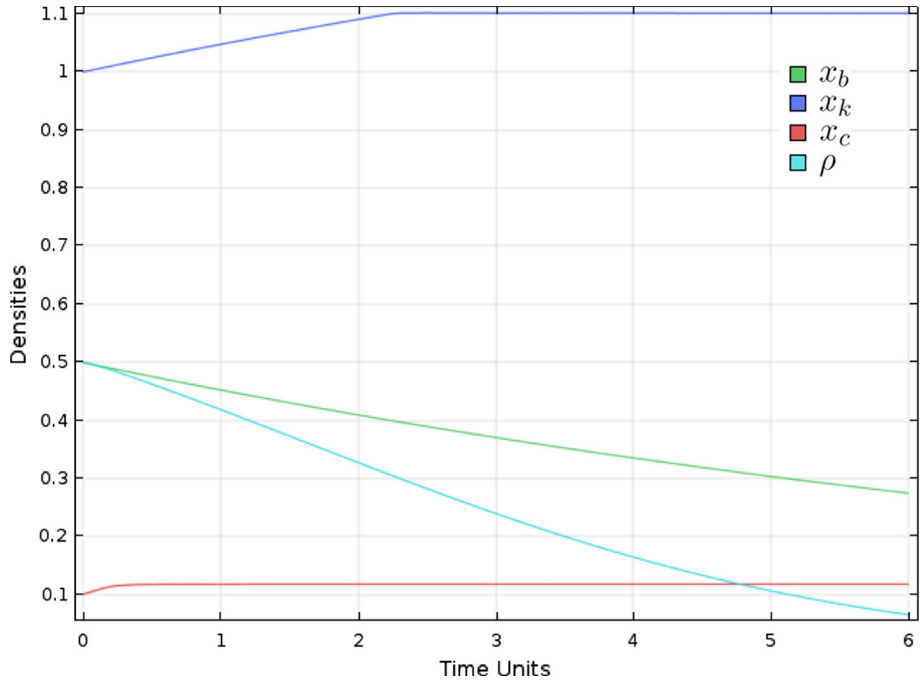

FIG. 7. The same simulation as in Fig.6, but this time with $\mathcal{K} \equiv 1$. In green is shown the osteoblasts density, in blue the osteocytes density, in red the osteoclasts density and in cyan the bone tissue density. It can be seen that there is a faster decrease of ρ but a faster increase of the osteocytes density (color figure online)

Summarizing, the proposed model consists of ODEs (1–4) and of balance equations (16) and (17), recalling that the energy density U depends on ρ through equation (15), while the stimulus S appearing in Eqs. (1–3) depends on U.

2.6. Parameters and initial data

As already outlined in the previous paragraphs, the complexity of the phenomena investigated, requires a large number of constitutive parameters, in order to model both the mechanical and the biological behavior. The initial values used for the numerical simulations shown later are here indicated. They do not have experimental confirmation, and for some of them (in particular parameter η) it is even difficult to imagine an experimental procedure which is capable of estimating it. Therefore, the values given here are to be considered provisional and chosen in order to capture the qualitative behavior in the largest possible set of different cases. All the parameters are dimensionless. Future investigation will be devoted to the proper parametrization of the model. The values used are indicated in the following table:

$a = 1$	$b = 7$	$S_0 = 0.6$	$\rho_0 = 0.5$
$x_{k0} = 1$	$x_{b0} = 0.5$	$x_{c0} = 0.1$	$\eta = 1000$
$\beta_k = 20$	$\beta_b = 20$	$\beta_c = 10$	$\alpha_b = 0.03$
$\gamma_{bk} = 0.1$	$\gamma_c = 0.1$	$\alpha_c = 0.1$	$\tilde{x}_k = 1.1$
$\tilde{x}_c = 0.11$	$\tilde{x}_b = 0.75$	$Y_m = 1$	$\nu = 0.15$
$D = 0.02$	$L = 1$	$l = 0.2$	$c = 2$

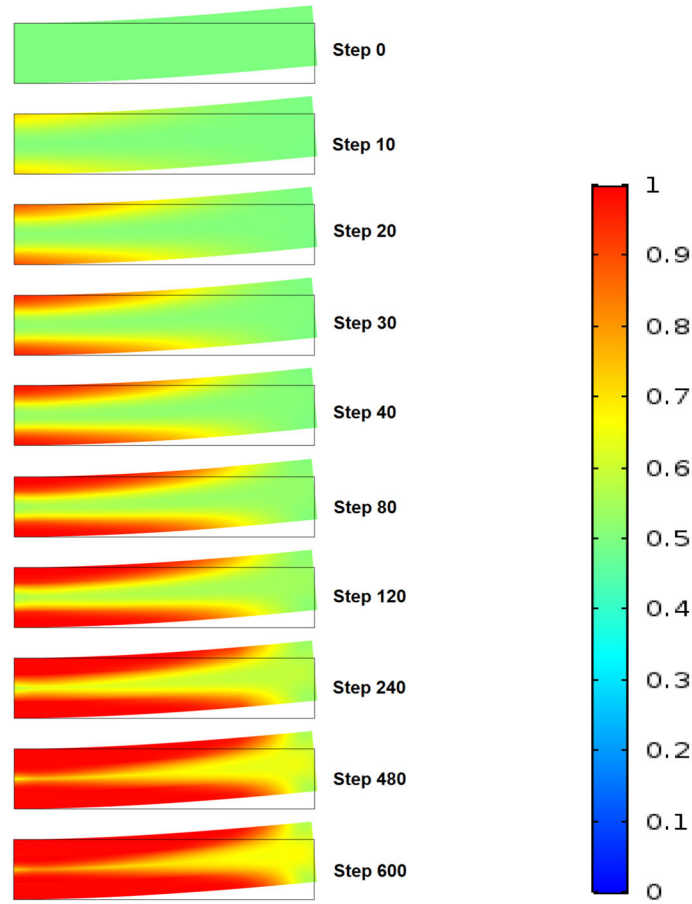

FIG. 8. A rectangular bone sample under a bending test. In color map, the (apparent) density of bone tissue is indicated. It can be seen that the density increases along the external portion of the sample (color figure online)

Here, Ymb is the maximum possible value for the Young modulus (set at 1), ν is the Poisson ratio, L and l are the normalized length and the height of the sample of considered bone tissue.

3. Numerical results

In this section, we will show numerical simulations of the behavior of the model presented in the previous part of the paper. The bone sample which will be considered is a rectangle, and we will show the effects of the application of constant loads. In all simulations, we considered clamped the left side of the sample, while the load is applied on the right side. A bidimensional example has been considered at this stage of the investigation as a good compromise between numerical costs and predicting ability. Indeed, these rectangular samples can be considered as sections of symmetric bodies, like cylindrical bones.

The model has been simulated using the mathematical library of Comsol Multiphysics (Weak Form and ODE): FEM has been employed to build and solve discrete systems of algebraic equations. In particular, for the mechanical content Hermite elements with third-order polynomials have been used, whereas the ODE system has been solved using the backward differentiation formula, with a variable order depending on the accuracy required.

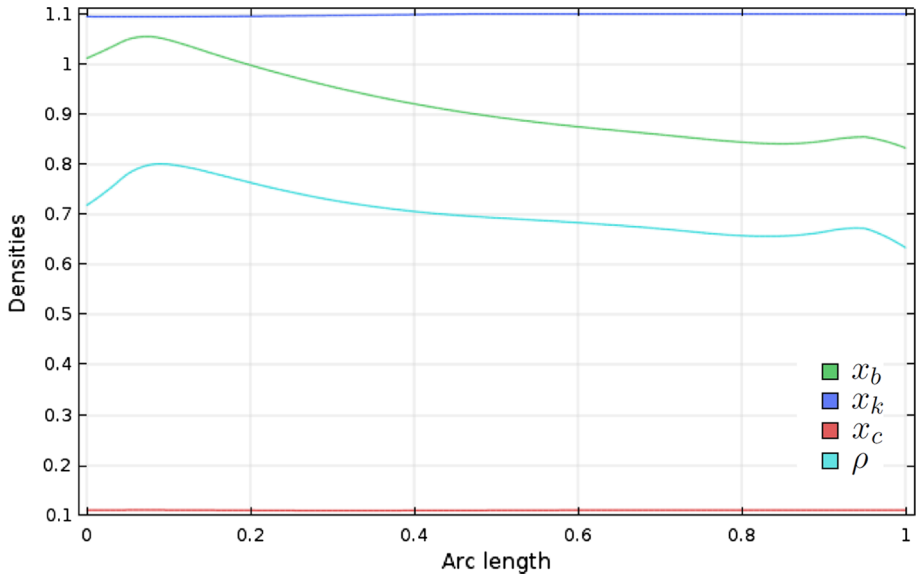

FIG. 9. Cell populations dynamics and density for a rectangular bone sample under a bending test. The values of the variables are evaluated at $t = 600$ along a central cut-line representing the neutral axis for the given bending test. In red is shown the osteoclasts density, in blue the osteocytes density, in green the osteoblasts density and in cyan the bone tissue density (color figure online)

3.1. Simple load

In the first simulations, we will apply a dimensionless compressive load orthogonal to the clamped side of the sample. The load is constant in time and large enough to make positive the stimulus (Its modulus is set at 1). The model can simulate the physiological increase of density in the bone tissue as a consequence of this external action. The initial values were uniform over all the sample and are given in section 2.6. As expected, the load leads to an increase of the apparent bone mass density (see fig. 2), a strong initial boost of osteoblasts density and an increase of osteocytes densities (see Fig. 3), while the osteoclast density has very small changes. Therefore, this simulation is compatible with the physiological behavior of the bone tissue.

3.2. Absence of loading

In absence of loading, the stimulus S is always negative. This promotes the osteoclasts genesis and therefore the bone tissue resorption, as shown in Fig. 5. The corresponding behavior of the cell populations (evaluated at the central point of the sample) is shown in Fig. 6, while the same simulation with $\mathcal{K}(\rho) \equiv 1$ is shown in Fig. 7. This means that the amount of porosity has less effect on the cell populations dynamics and leads to a faster decrease of ρ but a faster increase of the osteocytes density. The behavior of osteocytes deserves some comments. According to biological literature, liberated osteocytes die, or in some occasion can escape from the lacunae, after which it is still not completely clear what they can do. However, in the model there is no attempt at simulating this complex pathological process, as the main focus is the description of normal physiology. Therefore, below a certain threshold in the bone density the system (1–4) will need to be adapted in future studies.

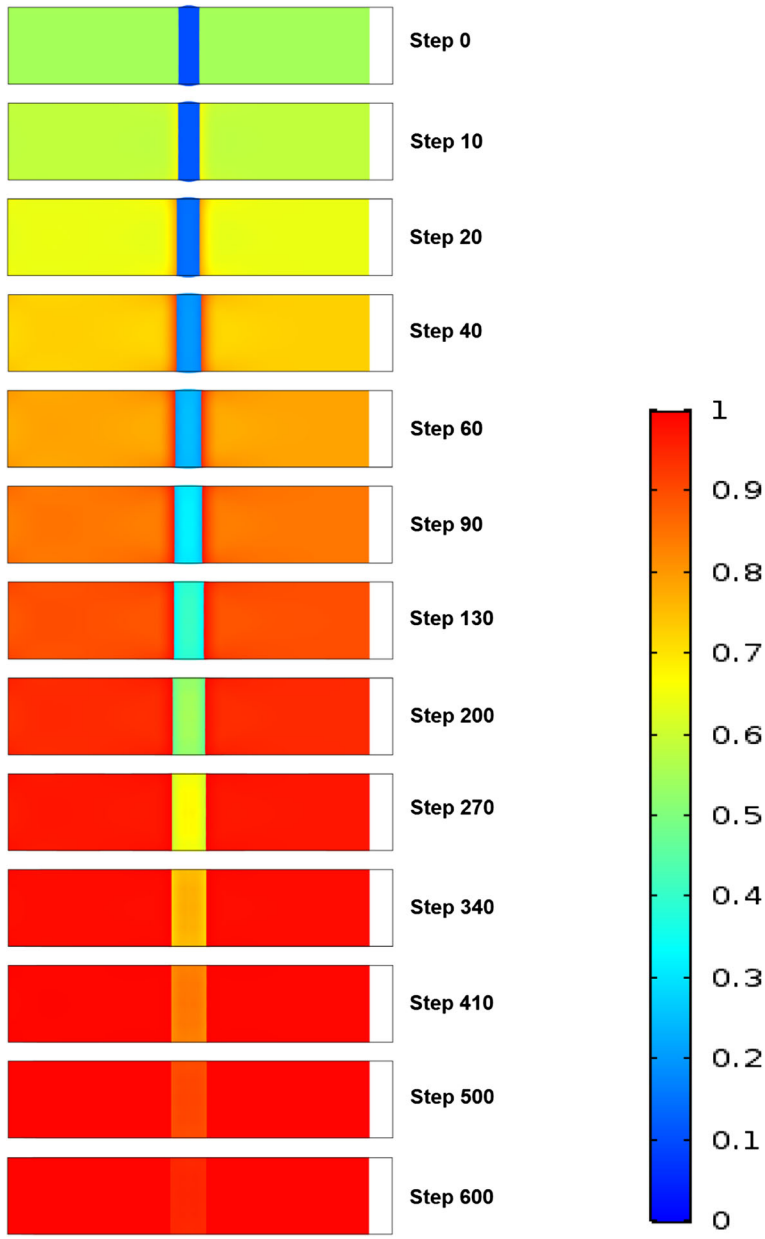

FIG. 10. A rectangular bone sample with a central fracture zone under simple compressive load. In color map, the (apparent) density of bone tissue is indicated. The external rectangle represents the unstressed configuration of the sample (color figure online)

3.3. Bending test

Here, we consider a simple bending test, in which the left side of the rectangular sample is clamped, while on the opposite side there is a (linear) distribution of forces producing a roto-translation. The corresponding simulation, with bone tissue density in color map, is shown in Fig. 8. It can be seen that

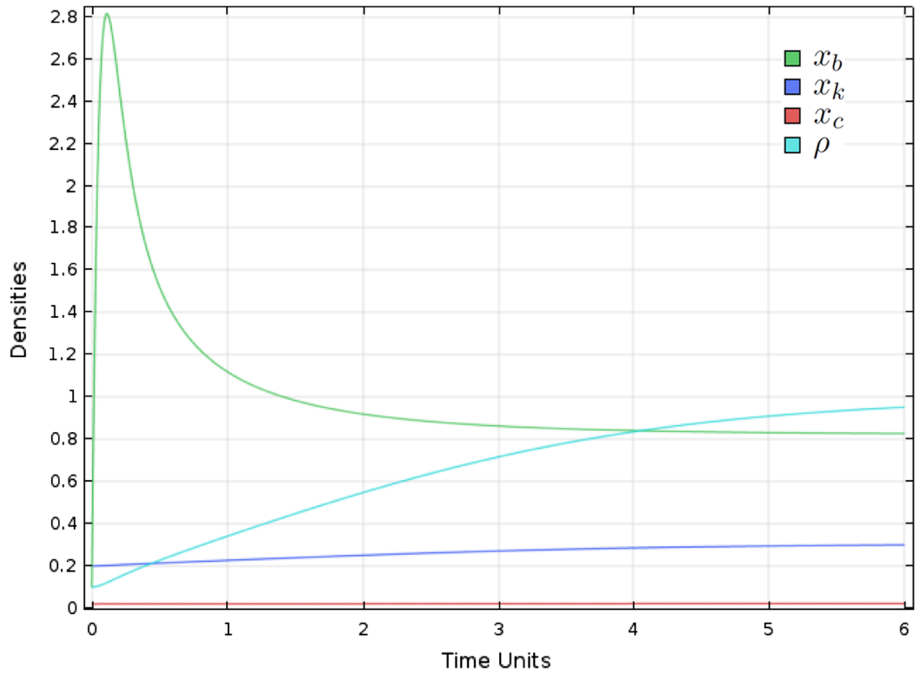

FIG. 11. Cell populations dynamics and density for a rectangular bone sample with a central fracture zone under simple compressive load. The values of the variables are evaluated at the central point of the sample. The picture shows the time history of the cell densities and bone tissue density. In green is shown the osteoblasts density, in blue the osteocytes density, in red the osteoclasts density and in cyan the bone tissue density (color figure online)

the density gradually increases along the external portion of the sample (Over a very long period, the density tends to become larger also in the central region). This is due to the fact that the deformation energy becomes larger when going far from the center neutral axis. As a consequence, the stimulus S becomes then larger, which gives in turn a higher production rate of osteoblasts. In Fig. 9, the cell populations densities along a central cut-line representing the neutral axis of the bending test are shown. As in that region there is very limited deformation energy, the stimulus is small and the cells densities are quite homogeneous and relatively low when compared to the external region. The simulations are in good agreement with normal physiological results.

3.4. Fracture healing test

In this section, we want to model the physiological healing of a small fracture and the related evolution of cell populations. We model the fracture zone in the bone sample as a region with negligible density. The model is able to simulate the healing in a reasonable way, as shown in Fig. 10. It can be noticed an increment of apparent bone tissue density at first outside the fracture zone, and then inside, a phenomenon which is related to the initial low density of osteocytes in the interested region. We used the following initial densities:

$$x_{i0}(x) = \begin{cases} x_{i0} & \text{if } 0 \leqslant x \leqslant 0.45L \\ \frac{x_{i0}}{10} & \text{if } 0.45L < x < 0.55L \\ x_{i0} & \text{if } 0.55 \leqslant x \leqslant L \end{cases}$$
$$i = k, b, c.$$

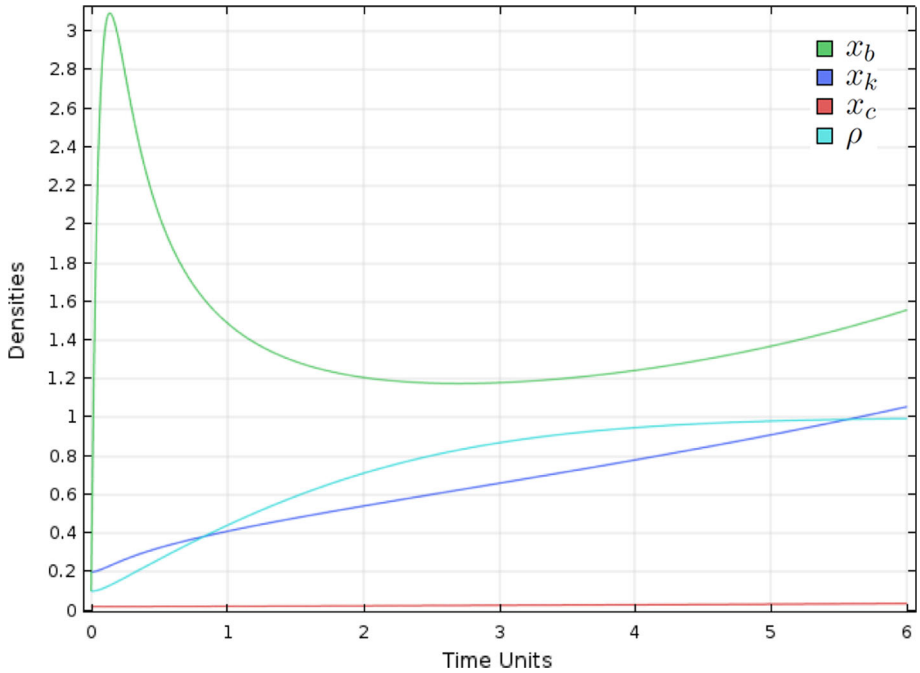

FIG. 12. The same simulation as in Fig. 11, but this time with $\mathcal{K} \equiv 1$. In green is shown the osteoblasts density, in blue the osteocytes density, in red the osteoclasts density and in cyan the bone tissue density (color figure online)

$$\rho_0(x) = \begin{cases} \rho_0 & \text{if } 0 \leqslant x \leqslant 0.45L \\ \frac{\rho_0}{10} & \text{if } 0.45L < x < 0.55L \\ \rho_0 & \text{if} 0.55 \leqslant x \leqslant L \end{cases}$$

Dimensionless load used has modulus equal to 1.

In Fig. 11, cell populations densities and bone tissue density, evaluated in the fracture zone, are shown. The initial peak of osteoblasts density is compatible with well-known physiological data. The model seems capable of describing the increase of the apparent density of the bone tissue. The density of osteocytes also increases, but rather slowly with $\mathcal{K} = 4(1-\rho)\rho$, while the same simulation with $\mathcal{K} \equiv 1$ (see Fig. 12) better describes the osteocytes repopulation phase. These results are useful to understand what the model can do, but it will be necessary to describe more accurately the fracture from a mechanical point of view, if one wants to obtain more realistic outputs (interesting in this direction are the results shown, e.g., in [16,46,47,49], and the applications in [36,43,44,52,56]).

4. Conclusions

In this paper, we presented a model for the description of bone physiology that couples a variational mechanical model with an ODEs system accounting for cell populations dynamics. The model we presented is able to describe qualitatively the principal features and behaviors of a bone tissue and relative cell populations dynamics in case of different loads as well as small fracture healing processes. Motivated by the present results, further refinements of the model are required in the following aspects:

- Evaluation of the parameters of the model according to experimental data.

- Inclusion of the possibility of cell migration, using a suitable diffusion tensor (see [11,26,53]).
- Adaptation of the model in case of very low density, especially for what concerns the behavior of osteocytes.
- Introduction of more general continuum models [12,42,54] and of the possibility of large deformations [14,22,32,45,55].
- The study of the dynamical behavior of bone tissue.

The latter is especially interesting as experimental results have shown that high-frequency stimulation can enhance significantly bone formation (see [15]). Therefore, the study of the dynamic behavior, including the analysis of the dynamical stability to ensure the safety of the therapeutic mechanical stimulation (see [18,37–39] for interesting results), can be of great importance in the future.

References

[1] Abali, B.E., Müller, W.H., Dell'Isola, F.: Theory and computation of higher gradient elasticity theories based on action principles. Arch. Appl. Mech. **87**, 1–16 (2017)
[2] Alibert, J.-J., Seppecher, P., dell'Isola, F.: Truss modular beams with deformation energy depending on higher displacement gradients. Math. Mech. Solids **8**(1), 51–73 (2003)
[3] Altenbach, H., Eremeyev, V.: Analysis of the viscoelastic behavior of plates made of functionally graded materials. ZAMM-J. Appl. Math. Mech./Zeitschrift für Angewandte Mathematik und Mechanik **88**(5), 332–341 (2008)
[4] Altenbach, H., Eremeyev, V.: On the constitutive equations of viscoelastic micropolar plates and shells of differential type. Math. Mech. Complex Syst. **3**(3), 273–283 (2015)
[5] Ambrosi, D., Ateshian, G.A., Arruda, E.M., Cowin, S.C., Dumais, J., Goriely, A., Holzapfel, G.A., Humphrey, J.D., Kemkemer, R., Kuhl, E.: Perspectives on biological growth and remodeling. J. Mech. Phys. Solids **59**(4), 863–883 (2011)
[6] Andreaus, U., dell'Isola, F., Giorgio, I., Placidi, L., Lekszycki, T., Rizzi, N.L.: Numerical simulations of classical problems in two-dimensional (non) linear second gradient elasticity. Int. J. Eng. Sci. **108**, 34–50 (2016)
[7] Andreaus, U., Giorgio, I., Lekszycki, T.: A 2D continuum model of a mixture of bone tissue and bio-resorbable material for simulating mass density redistribution under load slowly variable in time. Zeitschrift für Angewandte Mathematik und Mechanik **13**, 7 (2013)
[8] Andreaus, U., Giorgio, I., Madeo, A.: Modeling of the interaction between bone tissue and resorbable biomaterial as linear elastic materials with voids. Zeitschrift für angewandte Mathematik und Physik **66**(1), 209–237 (2014)
[9] Auffray, N., dell'Isola, F., Eremeyev, V., Madeo, A., Rosi, G.: Analytical continuum mechanics à la Hamilton–Piola least action principle for second gradient continua and capillary fluids. Math. Mech. Solids **20**(4), 375–417 (2015)
[10] Barchiesi, E., Placidi, L.: A review on models for the 3D statics and 2D dynamics of pantographic fabrics. In: Sumbatyan, M.A. (ed.) Wave Dynamics and Composite Mechanics for Microstructured Materials and Metamaterials, pp. 239–258. Springer, Berlin (2017)
[11] Bednarczyk, E., Lekszycki, T.: A novel mathematical model for growth of capillaries and nutrient supply with application to prediction of osteophyte onset. Zeitschrift für angewandte Mathematik und Physik **67**(4), 94 (2016)
[12] Bertram, A., Glüge, R.: Gradient materials with internal constraints. Math. Mech. Complex Syst. **4**(1), 1–15 (2016)
[13] Boutin, C., Giorgio, I., Placidi, L., et al.: Linear pantographic sheets: asymptotic micro-macro models identification. Math. Mech. Complex Syst. **5**(2), 127–162 (2017)
[14] Chatzigeorgiou, G., Javili, A., Steinmann, P.: Unified magnetomechanical homogenization framework with application to magnetorheological elastomers. Math. Mech. Solids **19**(2), 193–211 (2014)
[15] Clinton, T., Lanyon, L.E.: Regulation of bone formation by applied dynamic loads. J. Bone Joint Surg. Am. **66**, 397–402 (1984)
[16] Cuomo, M., Contrafatto, L., Greco, L.: A variational model based on isogeometric interpolation for the analysis of cracked bodies. Int. J. Eng. Sci. **80**, 173–188 (2014)
[17] Dallas, S.L., Bonewald, L.F.: Dynamics of the transition from osteoblast to osteocyte. Ann. N. Y. Acad. Sci. **1192**(1), 437–443 (2010)
[18] D'Annibale, F., Rosi, G., Luongo, A.: Linear stability of piezoelectric-controlled discrete mechanical systems under nonconservative positional forces. Meccanica **50**(3), 825–839 (2015)

[19] Della Corte, A.: Modeling synthesis and resorption phenomena in bones by means of mixture models enhanced with computational population dynamics. Part 2: models of bone cells population dynamics. In: France–Italy Workshop Bone Biomechanics: Multiscale and Multiphysical Aspects, Giuliano di Roma, Italy, 26–28 September (2017)
[20] Dell'Isola, F., Andreaus, U., Placidi, L.: At the origins and in the vanguard of peridynamics, non-local and higher-gradient continuum mechanics: an underestimated and still topical contribution of gabrio piola. Math. Mech. Solids **20**(8), 887–928 (2015)
[21] Dell'Isola, F., Della Corte, A., Giorgio, I.: Higher-gradient continua: the legacy of Piola, Mindlin, Sedov and Toupin and some future research perspectives. Math. Mech. Solids **22**(4), 852–872 (2017)
[22] Dell'Isola, F, Giorgio, I., Pawlikowski, M., Rizzi, N.: Large deformations of planar extensible beams and pantographic lattices: heuristic homogenization, experimental and numerical examples of equilibrium. In: Proceedings of the Royal Society, vol. 472, p. 20150790. The Royal Society, London (2016)
[23] Dell'Isola F, Seppecher P, et al (2018) Pantographic metamaterials: an example of mathematically driven design and of its technological challenges. Contin. Mech. Thermodyn. https://doi.org/10.1007/s00161-018-0689-8
[24] Eremeyev, V.A., Pietraszkiewicz, W.: Material symmetry group and constitutive equations of micropolar anisotropic elastic solids. Math. Mech. Solids **21**(2), 210–221 (2016)
[25] Franciosi, P., Spagnuolo, M., Salman, O.U.: Mean Green operators of deformable fiber networks embedded in a compliant matrix and property estimates. Contin. Mech. Thermodyn. 1–32 (2018) https://doi.org/10.1007/s00161-018-0668-0
[26] George, D., Allena, R., Remond, Y.: Cell nutriments and motility for mechanobiological bone remodeling in the context of orthodontic periodontal ligament deformation. J. Cell. Immunother. **4**(1), 26–29 (2018)
[27] Giorgio, I., Andreaus, U., dell'Isola, F., Lekszycki, T.: Viscous second gradient porous materials for bones reconstructed with bio-resorbable grafts. Extreme Mech. Lett. **13**, 141–147 (2017)
[28] Giorgio, I., Andreaus, U., Scerrato, D., dell'Isola, F.: A visco-poroelastic model of functional adaptation in bones reconstructed with bio-resorbable materials. Biomech. Model. Mechanobiol. **15**(5), 1325–1343 (2016)
[29] Goda, I., Assidi, M., Belouettar, S., Ganghoffer, J.F.: A micropolar anisotropic constitutive model of cancellous bone from discrete homogenization. J. Mech. Behav. Biomed. Mater. **16**, 87–108 (2012)
[30] Goda, I., Assidi, M., Ganghoffer, J.F.: Cosserat 3D anisotropic models of trabecular bone from the homogenisation of the trabecular structure. Comput. Methods Biomech. Biomed. Eng. **15**(sup1), 288–290 (2012)
[31] Graham, J.M., Ayati, B.P., Holstein, S.A., Martin, J.A.: The role of osteocytes in targeted bone remodeling: a mathematical model. PLoS ONE **8**(5), e63884 (2013)
[32] Greco, L., Cuomo, M., Contrafatto, L.: A reconstructed local $\bar{B}$ formulation for isogeometric *k*irchhoff-*l*ove shells. Comput. Methods Appl. Mech. Eng. **332**, 462–487 (2018)
[33] Greve, R., Placidi, L., Seddik, H.: A continuum-mechanical model for the flow of anisotropic polar ice. Contin. Mech. Thermodyn. **22**, 221–237 (2010)
[34] Komarova, S.V., Smith, R.J., Dixon, S.J., Sims, S.M., Wahl, L.M.: Mathematical model predicts a critical role for osteoclast autocrine regulation in the control of bone remodeling. Bone **33**(2), 206–215 (2003)
[35] Lekszycki, T., dell'Isola, F.: A mixture model with evolving mass densities for describing synthesis and resorption phenomena in bones reconstructed with bio-resorbable materials. ZAMM-Zeitschrift für Angewandte Mathematik und Mechanik **92**(6), 426–444 (2012)
[36] Lu, Y., Lekszycki, T.: Modelling of bone fracture healing: influence of gap size and angiogenesis into bioresorbable bone substitute. Math. Mech. Solids **22**(10), 1997–2010 (2017)
[37] Luongo, A., D'Annibale, F.: Double zero bifurcation of non-linear viscoelastic beams under conservative and non-conservative loads. Int. J. Non-Linear Mech. **55**, 128–139 (2013)
[38] Luongo, A., D'Annibale, F., Ferretti, M.: Hard loss of stability of Ziegler's column with nonlinear damping. Meccanica **51**(11), 2647–2663 (2016)
[39] Luongo, A., Piccardo, G.: Linear instability mechanisms for coupled translational galloping. J. Sound Vib. **288**(4–5), 1027–1047 (2013)
[40] Melnik, A.V., Goriely, A.: Dynamic fiber reorientation in a fiber-reinforced hyperelastic material. Math. Mech. Solids **18**(6), 634–648 (2013)
[41] Milton, G., Briane, M., Harutyunyan, D.: On the possible effective elasticity tensors of 2-dimensional and 3-dimensional printed materials. Math. Mech. Complex Syst. **5**(1), 41–94 (2017)
[42] Mindlin, R.D., Tiersten, H.F.: Effects of couple-stresses in linear elasticity. Arch. Ration. Mech. Anal. **11**(1), 415–448 (1962)
[43] Misra, A., Poorsolhjouy, P.: Granular micromechanics model for damage and plasticity of cementitious materials based upon thermomechanics. Math. Mech. Solids, (2015) https://doi.org/10.1177/1081286515576821
[44] Misra, A., Poorsolhjouy, P.: Identification of higher-order elastic constants for grain assemblies based upon granular micromechanics. Math. Mech. Complex Syst. **3**(3), 285–308 (2015)
[45] Ogden, R.W.: Large deformation isotropic elasticity-on the correlation of theory and experiment for incompressible rubberlike solids. In: Proceedings of the Royal Society of London A: Mathematical, Physical and Engineering Sciences, vol. 326, pp. 565–584. The Royal Society, London (1972)

[46] Placidi, L., Barchiesi, E.: Energy approach to brittle fracture in strain-gradient modelling. Proc. R. Soc. A **474**(2210), 20170878 (2018)
[47] Placidi, L., Barchiesi, E., Misra, A.: A strain gradient variational approach to damage: a comparison with damage gradient models and numerical results. Math. Mech. Complex Syst. **6**(2), 77–100 (2018)
[48] Placidi, L., Greve, R., Seddik, H., Faria, S.: Continuum-mechanical, anisotropic flow model for polar ice masses, based on an anisotropic flow enhancement factor. Contin. Mech. Thermodyn. **22**(3), 221–237 (2010)
[49] Placidi, L., Misra, A., Barchiesi, E.: Two-dimensional strain gradient damage modeling: a variational approach. Zeitschrift für angewandte Mathematik und Physik **69**(3), 56 (2018)
[50] Ren, Y., Feng, J.Q.: Osteocytes play a key role in the formation and maintenance of mineralized bone. FASEB J. **31**(1–supplement), 7-1 (2017)
[51] Robling, A.: Osteocytes orchestrate mechanical signal transduction in bone via WNT. FASEB J. **31**(1–supplement), 7-3 (2017)
[52] Rosi, G., Placidi, L., Auffray, N.: On the validity range of strain-gradient elasticity: a mixed static-dynamic identification procedure. Eur. J. Mech.-A/Solids **69**, 179–191 (2018)
[53] Spingarn, C., Wagner, D., Remond, Y., George, D.: Theoretical numerical modeling of the oxygen diffusion effects within the periodontal ligament for orthodontic tooth displacement. J. Cell. Immunother. **4**, 44 (2018)
[54] Toupin, R.A.: Elastic materials with couple-stresses. Arch. Ration. Mech. Anal. **11**(1), 385–414 (1962)
[55] Turco, E., Golaszewski, M., Cazzani, A., Rizzi, N.L.: Large deformations induced in planar pantographic sheets by loads applied on fibers: experimental validation of a discrete lagrangian model. Mech. Res. Commun. **76**, 51–56 (2016)
[56] Turco, E., Dell'Isola, F., Rizzi, N.L., Grygoruk, R., Müller, W.H., Liebold, C.: Fiber rupture in sheared planar pantographic sheets: numerical and experimental evidence. Mech. Res. Commun. **76**, 86–90 (2016)

Alessio Ciro Rapisarda
University of Naples Federico II
Naples
Italy

Alessandro Della Corte and Fabio Di Cosmo
International Research Center for the Mathematics and Mechanics of complex Systems (M&MoCS)
University of L'Aquila
L'Aquila
Italy
e-mail: fabio.dicosmo.memocs@gmail.com

Rafał Drobnicki
Dipartimento di Ingegneria e Scienze dell'Informazione e Matematica
Università degli Studi dell'Aquila
Via Vetoio, Coppito
67100 L'Aquila
Italy

Luigi Rosa
Dipartimento di Matematica e Applicazioni Renato Caccioppoli
University of Naples Federico II
Naples
Italy

(Received: October 10, 2018; revised: November 18, 2018)